Erschienen in: Journal of Structural Biology ; 199 (2017), 1. - S. 46-56
https://dx.doi.org/10.1016/j.jsb.2017.05.004

Retrosynthesis of $CaCO_3$ via amorphous precursor particles using gastroliths of the Red Claw lobster (*Cherax quadricarinatus*)

Andrónico Neira-Carrillo [a,*], María Soledad Fernández [a], Gonzalo Poblete Hevia [a], José Luis Arias [a], Denis Gebauer [b], Helmut Cölfen [b]

[a] Faculty of Veterinary and Animal Sciences, University of Chile, Santiago, Chile
[b] Department of Chemistry, University of Konstanz, Konstanz 78464, Germany

A B S T R A C T

Gastroliths are highly calcified structures formed in the cardiac stomach wall of crustaceans for the temporary storage of amorphous $CaCO_3$ (ACC). The gastrolithic ACC is stabilized by the presence of biomolecules, and represents a novel model for research into biomineralization. For the first time, an *in vitro* biomimetic retrosynthesis of scaffolds of gastrolithic matrices with $CaCO_3$ is presented. With the help of synthetic polyacrylic (PAA) and phytic (PA) acids, amorphous precursor particles were stabilized in double (DD) and gas (GD) diffusion crystallization assays. The presence of these synthetic molecules as efficient inhibitors of nucleation and growth of $CaCO_3$, and the use of biological gastrolith scaffolds as confined reaction environments determined the kinetics of crystallization, and controlled the morphogenesis of $CaCO_3$. The formation of ACC particles was demonstrated and their crystallization was followed by light microscopy, scanning and transmission electron microscopy, and electron diffraction.

1. Introduction

Living organisms produce and biologically control the formation of inorganic-organic composites materials and control the inorganic reactions forming mineral assemblages (Lowenstam and Weiner, 1989; Mann, 2001a,b). This biological mineralization phenomenon, known as biomineralization, has offered outstanding examples for controlling mineral deposition in the range of nanometer to micrometer scales, occurring widespread from bacteria to mammals (Mann, 2001a,b; Mann and Ozin, 1996; Ozin, 1997). Biominerals often exhibit highly sophisticated structural features such as sea- and eggshells, exoskeletons of corals, crustacean carapaces, coccoliths, teeth and bones in mammals, among others (Lowenstam, 1986; Dove et al., 2003). The deposition of minerals within various biological tissues is a well-controlled inorganic process. Biominerals are organic/inorganic hybrid composite materials consisting of organic and mineral parts, subdivided into soluble and insoluble matrices. The organic parts, mostly proteins and polysaccharides, act as a biological template, where mostly organic acid-Ca^{2+} mineral interactions control the structure, shape and size of the composite material (Bäuerlein, 2003; Cölfen and Mann, 2003; Mann, 1996). The toughness of biominerals depends on both, the degree of mineralization and the type of mineral. Therefore, biomimetic approaches inspired by biomineralized structures have been explored for the development of novel materials (Lowenstam and Weiner, 1989; Mann, 2001a,b; Mann and Ozin, 1996; Ozin, 1997; Lowenstam, 1986; Dove et al., 2003).

In crustaceans, *e.g.* lobsters and crayfish, molting represents a continual and active physiological process (*ecdysis*), due to the indeterminate and cyclic growth of the carapace. Crayfish produce a reservoir of Ca^{2+} ions immediately available after ecdysis, called gastrolith. Gastroliths are highly calcified disc-shaped structures (2 or 4 per animal), cyclically formed in the cardiac stomach wall between a calcifying epithelium and a cuticle (Luquet and Marin, 2004), and grow daily during the premolt period and reach their maximum size just before molting (Shechter et al., 2008). The calcification process in crustaceans has led to the development of Ca-storage strategies (Travis, 1963). Calcium is stored mainly as amorphous $CaCO_3$ (ACC) (Bentov et al., 2010). $CaCO_3$ is the major inorganic mineral component of gastroliths, and presently represents one of the most studied biomineralization systems, which may improve our understanding of biological control on mineralization (Lowenstam and Weiner, 1989; Mann, 2001a,b; Mann and Ozin, 1996; Ozin, 1997; Meldrum, 2003; Cölfen, 2003). The formation process of $CaCO_3$ and the involved molecular mechanisms have been extensively investigated, due to its importance in both geological and biological settings. Therefore, controlled syntheses of ACC nanoparticles with regular morphology are of

* Corresponding author.

increasing interest due to their importance for the generation of organic/inorganic composites with superior materials properties with various potential applications (Meldrum, 2003; Pai and Pillai, 2008).

Among the most active additives that control biological mineralization are a group of unusually acidic proteins (P), proteoglycans (PG) and their associated glycosaminoglycans (GC). (Weiner and Addadi, 1991; Pereira-Mouriès et al., 2002) The polysaccharide components of PG are among the most acidic molecules in biological systems. GC are also anionic polysaccharides, consisting of repeating disaccharides of an amino sugar and another monosaccharide, which contain sulfate and carboxylic anionic groups (Yanagishita and Hascall, 1983; Arias et al., 1992, 2004)

Our previous research has indicated that the organic matrix of gastroliths contains PG, which have been suggested to play a role in the stabilization of ACC (Fernández et al., 2012; Arias and Fernández, 2008). Due to its relatively simple structure and rapid formation and dissolution, the gastrolith is a good biomineralization model for exploring the *in vitro* $CaCO_3$ retrosynthesis mineralization. As outlined above, the motivation for investigating the principles of biomineralization is their potential adaptability for growing synthetic analogues, here based on the amorphous precursor route employing gastrolith scaffold matrices. According to previous studies (Xu et al., 2005), the use of inositol hexakisphosphate (phytic acid, PA) could help to synthesize stable ACC with spherical hollow superstructures, demonstrating that the use of phosphorous groups of the PA not only can act as a crystallization inhibitor, but also as colloidal stabilizer. For instance, PA has been used as *in vitro* inhibitor for calcium oxalate crystallization and stone growth, demonstrating the calcium binding efficiency of phytate molecules (Saw et al., 2007).

2. Materials and methods

All reagents were of highest available grade, and bidestilled water was used for the preparation of all solutions. Gastroliths were obtained from pre-molted Red Claw Lobsters *Cherax quadricarinatus*. For the crystallization experiments based on the DD method utilizing PAA, the following reactants were used: Calcium chloride powder ($CaCl_2$, MW: 111.0 g/mol) from Sigma, sodium carbonate (Na_2CO_3, MW: 105.99 g/mol) from Aldrich and synthetic sodium acrylate from Fluka. The crystallization was based on the GD method. Calcium chloride ($CaCl_2$), ethanol, and tris(hydroxymethyl) aminomethane (TRIS) were obtained from ACS-Merck, and ammonium hydrogen carbonate (NH_4HCO_3) was from J.T. Baker. Deionized water was obtained from capsule filter 0.2 μm flow (U.S. Filter).

2.1. In vitro retrosynthesis of $CaCO_3$

For this study, 10 gastroliths were decalcified by immersion in 10% formic acid solution at 4 °C for 7 days. The solvent was exchanged to obtain the insoluble and soluble fractions (Fig. 1). The soluble fraction (SF) was obtained by dialyzing and lyophilizing the supernatant. The powdered SF was treated with 4 M guanidine chloride containing detergents and protease inhibitors to obtain a P and PG enriched fraction (Yanagishita and Hascall, 1983; Arias et al., 1992). This fraction was chromatographed over Sephadex G-50. The void volume was applied to a DEAE-Sephacel anion-exchange column to obtain a PG enriched FS fraction.

The insoluble fraction (IF) was treated with 4 M guanidine chloride containing detergents and protease inhibitors to remove PG (Yanagishita and Hascall, 1983; Arias et al., 1992). These PG-free IF referred to as gastrogel, was used for the *in vitro* retrosynthesis experiments. For the biomimetic mineralization of $CaCO_3$, both the GD and the DD methods were employed (Domínguez-Vera et al., 1999; Gehrke et al., 2005). For the retrosynthesis experiments of $CaCO_3$ based on the DD method, a solution of synthetic PAA was used for the stabilization of amorphous precursor particles. Briefly, 2L solutions of $CaCl_2$ (3.5 mM) and sodium carbonate (3.5 mM) containing 50 μg/ml PAA (Fluka, 5.100 g/mol) were used. In the DD method, both solutions were exchanged every day and the flow rate was 0.55 ml/min. Crystallization experiments were performed in a beaker (2L) that was filled with carbonate buffer (25 mL, 10 mM, with or without the particular additive), pH 9.75. $CaCl_2$ solution (3.5 mM) set to pH 9.75 (volume dilution due to pH-adjustment was considered) was dosed at a rate of 10 mL per minute. For experiments in presence of 50 μg/ml PAA, $CaCl_2$ (3.5 mM) solution set to pH 9.75 was added at a rate of 10 mL per minute, similar to crystallization experiments using carbonate buffer and $CaCl_2$ solution in the presence of PAA as additive where the pH was automatically maintained at a constant level (Volkmer et al., 2005; Gebauer et al., 2009). In the DD method, both solutions were exchanged every day and the flow rate was 0.55 ml/min. In the GD method, different gastrogel and sponge pieces as gastrolith matrices were placed in 10 mL of $CaCl_2$ solution (10 mM) containing PA (Aldrich, 660.04 AMU) as additive (1 g/L prepared from 40% (w/w) solution in water (Xu et al., 2005). Different disposable glass containers containing the solutions with the gastrolith matrices—and one with 7 g of ammonium carbonate (Fluka)—were covered with pinholed Parafilm and placed into a desiccator for certain amounts of time (15 min up to 2 months) at room temperature. Afterwards, matrix pieces were removed from the solution, washed with water, and dried. In addition, powders of the fraction obtained after demineralization of the gastroliths were also used as additive (10 wt%) in PA/$CaCl_2$ solution (Xu et al., 2005; Arias et al., 2004; Neira-Carrillo et al., 2009, 2012).

2.2. Characterization

For the retrosynthesis experiments of $CaCO_3$ through DD and GD methods, both light and scanning electron microscopy (SEM) were used to observe crystalline particle materials. The use of *in situ* light microscopy was necessary to corroborate that the SEM micrographs showed real structures instead of drying artifacts resulting from the sample preparation. Light microscopy images were taken in solution with an Olympus BX50 microscope. For the visualization of internal and external parts of the gastrogel matrix, a cryo-sectioned preparation was carried out. The SEM images were performed on a DSM940A (Carl Zeiss, Jena), and the pictures were taken with a digital camera connected to the SEM. In case of both crystallization methods, the specimens were directly taken from the solution. Transmission electron microscopy (TEM) and electron diffraction were performed on an EM 912 Ω (Zeiss) instrument. The diffraction spectrum was taken directly from samples using a Siemens D-5000 X-ray diffractometer with CuKα radiation (graphite monochromator). Wide-angle X-ray diffraction (WAXS) spectra were measured on a Bruker Vector 22 and an ENRAF Nonius FR 590 diffractometer with CuKα radiation, respectively.

3. Results and discussion

The gastroliths produced during the pre-molting stage in the cardiac stomach wall exhibit a semi-spherical morphology after ecdysis (Travis, 1963). Fig. 2 shows anatomically where the gastroliths are located in the lobster and different sizes of gastrolith stones, whereas their size is proportional to the size of adult specimens. Gastrolith concretions have a flat concave and convex sides related to their anatomical location in the stomach lumen. The

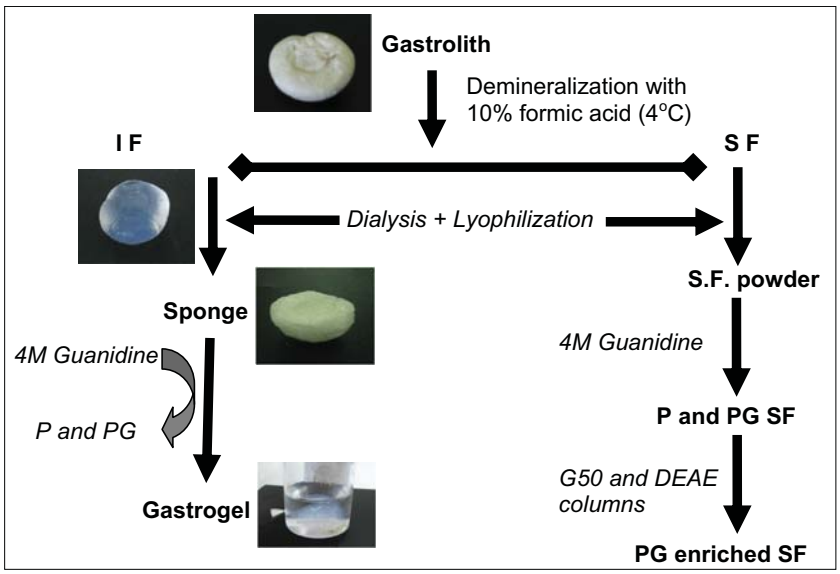

Fig. 1. Experimental procedure for the preparation of matrices of scaffold gastroliths. IF and SF indicate insoluble and soluble fractions, respectively. P and PG indicate proteins and proteoglycans, respectively.

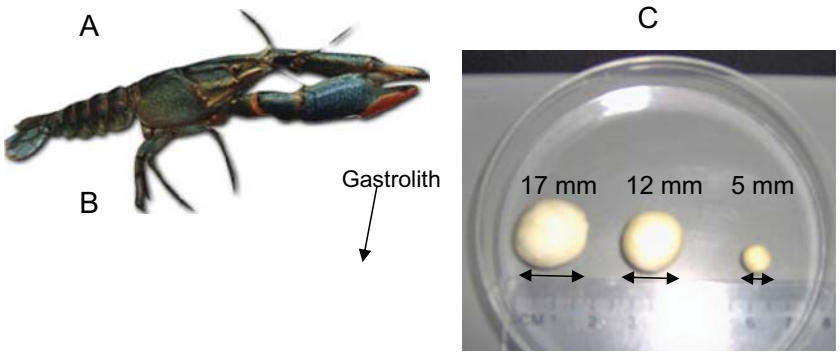

Fig. 2. Anatomical location of gastrolith stone in Red claw lobster (*Cherax quadricarinatus*) and size of gastroliths in the range of mm.

occurrence of PG molecules in gastroliths of the crayfish *Cherax quadricarinatus* and analyses of the ultrastructure and composition of gastroliths from freshwater crayfish utilizing a combination of microscopic and physical techniques have been previously reported (Fernández et al., 2012; Luquet et al., 2013).

The gastrolith scaffold matrices, which were used as solid substrates for the retrosynthetic crystallization assays, were employed according to the experimental procedure shown in Fig. 1. After demineralization of the gastroliths with 10% formic acid, the insoluble (IF) and soluble (SF) fractions were obtained. From the IF, the sponge scaffold was obtained after dialysis and lyophilization. Another scaffold was obtained from the IF - here referred to as gastrogel - after removal of P and PG molecules by applying 4 M guanidine and dialysis. The retrosynthetic mineralization performed in the presence of both gastrolith scaffolds as templates in GD and DD crystallization resulted in $CaCO_3$ particles with different crystal structures and morphologies.

The morphological appearance of both gastrolith scaffold matrices and the original gastrolith stone was analyzed by means of electron (Fig. 3A–D) and optical microscopy (Fig. 3E–F). The original gastrolith showed a multilayered organization (Fig. 3A). High magnification of the external part (Fig. 3B) of the gastrolith demonstrated the presence of regular spherical nanoparticles of $CaCO_3$ with a size of *ca.* 100 nm, probably surrounded by chitin fibers. Similar spherical nanoparticles of stabilized ACC as the main component of the Ca-storage structure have been also reported in organisms such as the terrestrial crustaceans *Orchestia cavimana* and *Porcellius scaber* (Raz et al., 2002; Ziegler, 1994; Fabritius et al., 2005). The gastrogel and sponge matrices obtained from the IF were also analyzed, and we expected distinct microstructures. Indeed, Fig. 3C shows the gastrogel matrix, which has a compact network appearance composed of interconnected fibers. With the naked eye, a transparent appearance of the gastrogel matrix is apparent, and the layered arrangement showed a similar macroscopic shape as the original gastrolith (Fig. 1). On the other hand, the sponge matrix (Fig. 3D) showed an irregular surface formed by overlapping "cornflake-like" structures after being treated by dialysis and lyophilization.

In order to evaluate the influence of the gastrolith scaffold matrices on the *in vitro* $CaCO_3$ crystallization in real time, a set of retrosynthesis mineralization experiments using both gastrolith matrices were performed varying the mineralization time at room temperature. Fig. 4 shows the $CaCO_3$ particle formation in real time on gastrogel (Fig. 4A) and sponge (Fig. 4B) as template scaffolds

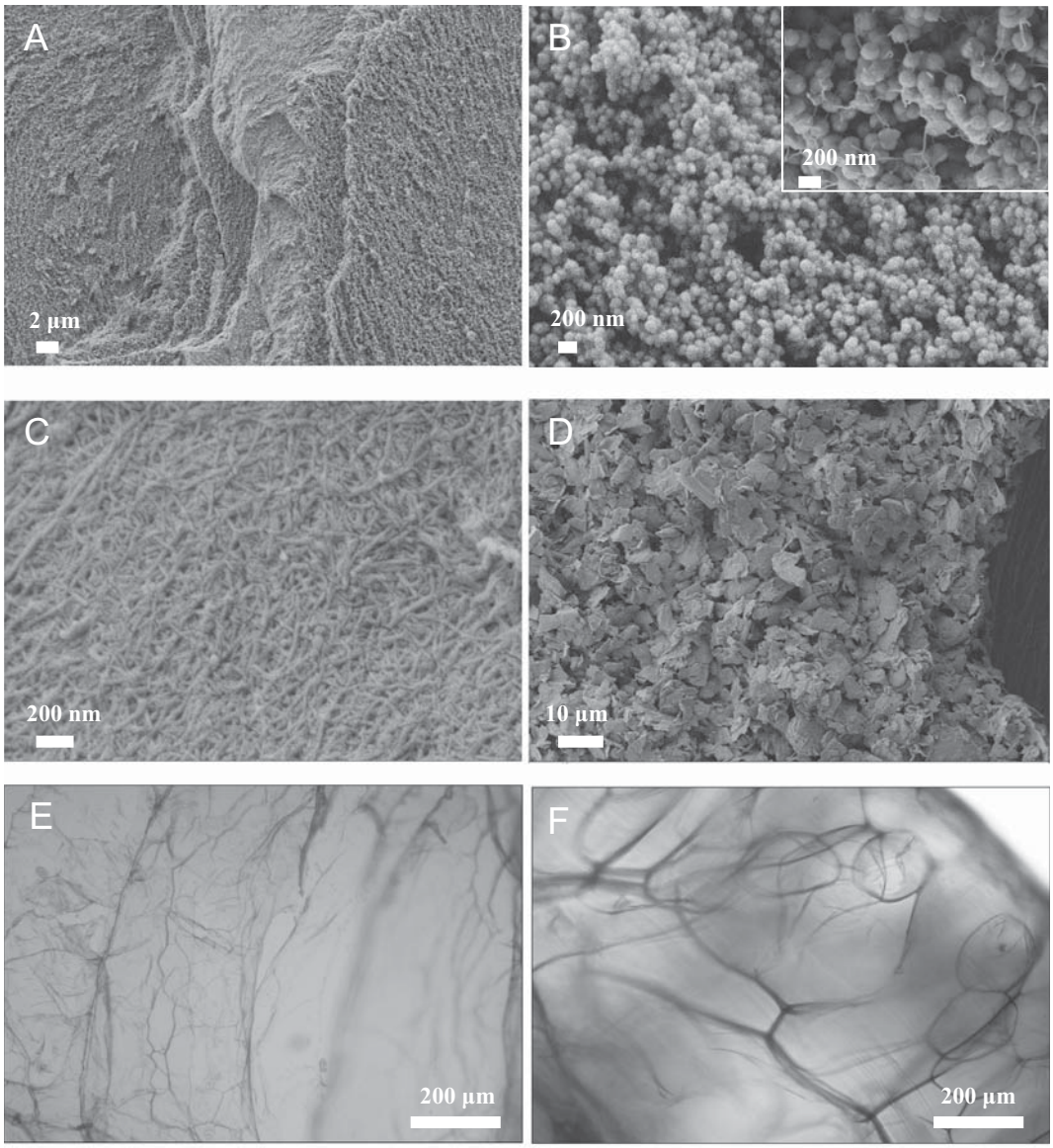

Fig. 3. SEM images of gastrolith scaffold matrices: A, B) gastrolith stone, C) gastrogel and D) sponge. Light microscopy of inner parts of: E) gastrogel and F) sponge using cryo-cut preparation at −20 °C.

through DD diffusion from 15 min to 8 days visualized by light microscopy. Although, there is no quantitative data on the nucleation and crystal growth rates of $CaCO_3$ mineralization, the light microscopy analysis show a remarkable difference in the relative density of $CaCO_3$ particles when both scaffold matrices were compared. Thus, a faster mineralization of $CaCO_3$ on the sponge matrix was observed at any time of the mineralization process, probably due to the presence of heterogeneous organic molecules and the complex mechanism of mineralization in exoskeleton and gastroliths concretion (Habraken et al., 2015). If nucleation was homogenous and the substrate matrices had no effect on this process, the relative density of $CaCO_3$ particles should be identical on both gastrolith matrices at any observed time. Since the relative density of $CaCO_3$ particles was always higher on the sponge matrix compared to gastrogel at the same time, we suggest that the presence of P and GP biomolecules facilitate heterogeneous crystallization of the solid substrate during retrosynthesis. Thus, a larger amount of $CaCO_3$ particles was observed from 6 h when the sponge substrate was used (Fig. 4I). Altogether, the light microscopy analyses reveal that the presence or absence of biological molecules contained in the gastrolith components as organic scaffold lead to different effects on $CaCO_3$ mineralization.

Alternatively, SEM analyses of $CaCO_3$ grown on both scaffold matrices through the DD crystallization method in the presence of PAA were performed (Fig. 5). Fig. 5 (A–D) shows the SEM images of $CaCO_3$ aggregate particles grown in two distinct zones of the gastrogel matrix, which show characteristic polycrystalline microparticles of $CaCO_3$ with spherical lumps (Fig. 5 A,B). The perpendicular flat growing face of $CaCO_3$ particles (Fig. 5 C,D) grown on the gastrogel surface suggests more than one type of retrosynthesis mineralization mechanisms. However, in Fig. 5 (E,F) when the sponge was used as the scaffold, the presence of organic biomolecules such as P and PG induces the formation of more abundant and regular $CaCO_3$ particles, and growth of nanoparticles into the layers of the sponge matrix. This indicates that organic biomolecules such as P, PG and other organic molecules reported

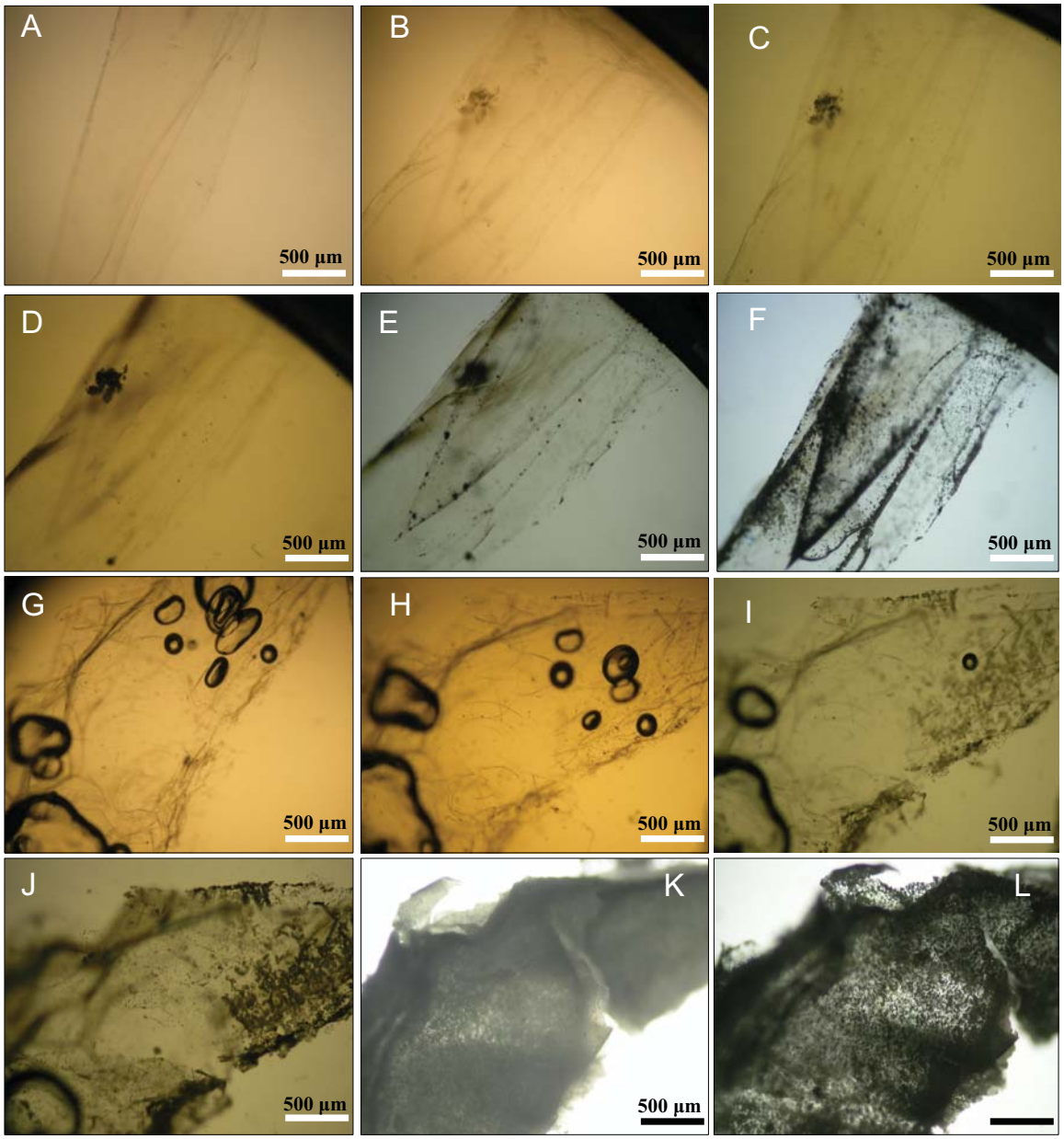

Fig. 4. Light microscopy visualizing in real time $CaCO_3$ particles in gastrolith matrices through DD diffusion from 15 min to 8 days: A–F) gastrogel, G–L) sponge. A) 15 min, B) 1 h, C) 6 h, D) 1 day, E) 4 days, F) 8 days, G) 15 min, H) 1 h, I) 6 h, J) 1 day, K) 4 days, L) 8 days.

to be present in scaffold matrices (Sato et al., 2011; Habraken et al., 2015; Luquet et al., 2016), play a crucial role in the $CaCO_3$ retrosynthetic mineralization process.

In order to investigate the influence of the ultrastructure of both gastrolith scaffold matrices involved during the DD retrosynthetic mineralization, TEM and electron diffraction measurements on both mineralized scaffold matrices and in the original gastrolith stone using PAA after 8 days at room temperature were performed (Fig. 6A–C). It is important to note that in case of the gastrogel, which was obtained after treating the sponge matrix with the 4 M guanidine chloride, the electron diffraction patterns of $CaCO_3$ particles showed circular diffraction patterns indicative of polycrystalline $CaCO_3$ particles (Fig. 6B2), however, there are intense arcs that suggest a certain preferential orientation. In case of the sponge matrix (Fig. 6C), obtained just after dialysis and lyophilization of the IF, the electron diffraction analysis indicates non-oriented polycrystalline aggregates without this feature (Fig. 6C2). All diffraction patterns are indicative of crystalline $CaCO_3$, presumably corresponding to calcite. Electron diffraction patterns of $CaCO_3$ particles grown on both scaffold matrices using PAA after 21 days at room temperature showed the same behavior indicating more oriented polycrystalline particles for the gastrogel instead of the sponge (Supporting information, Fig. S1).

The presence of P and PG biomolecules and other reported molecules such as phosphorous-containing compounds (Sato et al., 2011; Habraken et al., 2015), which stabilize ACC particles, also becomes evident in the current observations for PG-rich and PG-free gastrolith matrices, forming more or less oriented crystalline $CaCO_3$, respectively. This indicates that the molecules responsible for ACC stabilization in the gastrolith also have an effect on the crystallization in the mineralization experiments. In fact, the description of the *in situ* structural molecular characteriza-

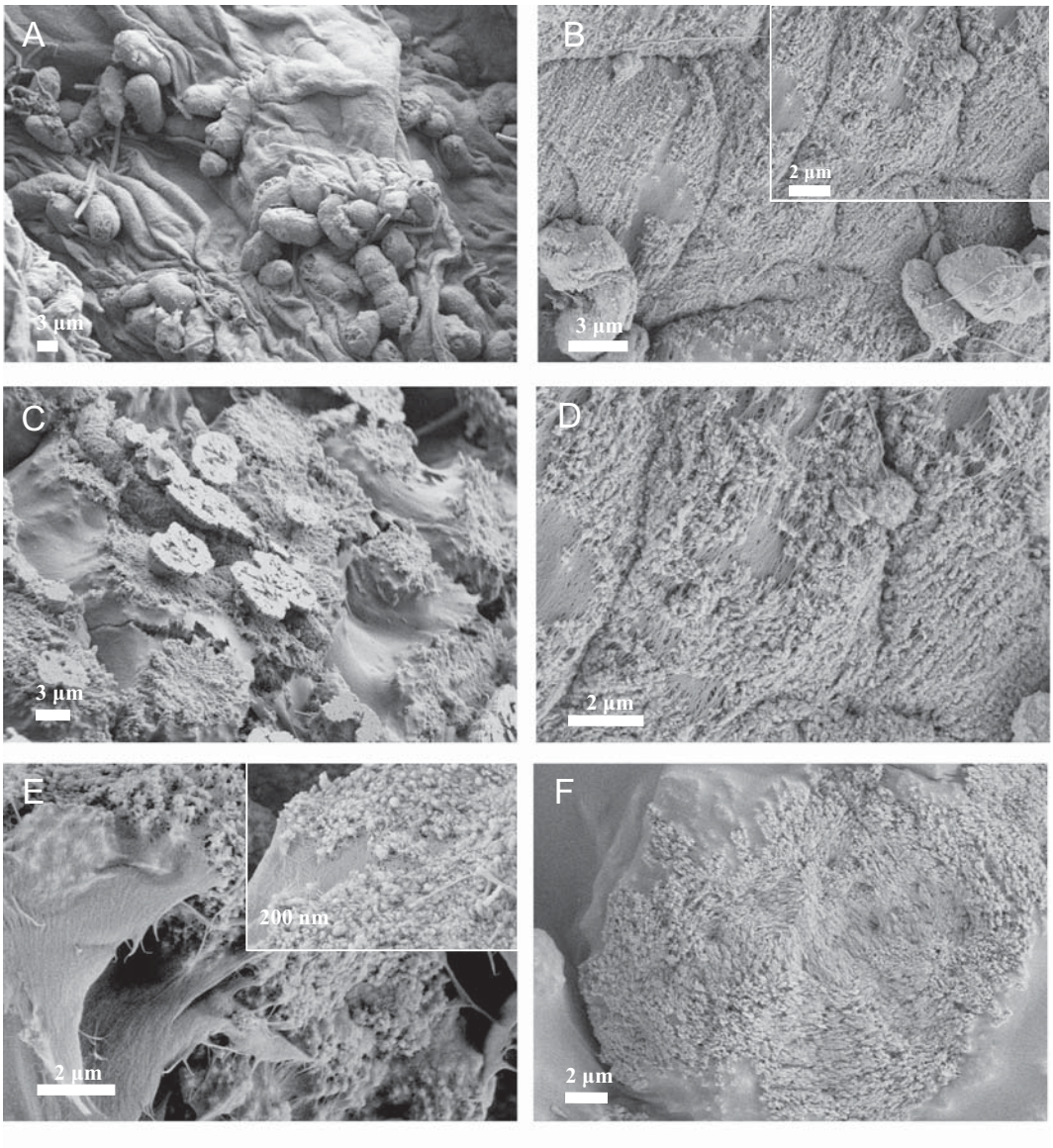

Fig. 5. SEM images of $CaCO_3$ particles grown using the DD method (Retrosynthesis) with PAA on A–D) gastrogel and E–F) sponge matrices.

tion of gastrolith ACC and the bioavailable Ca stabilized as ACC biomineral in crayfish gastrolith has been well documented by multinuclear NMR technique (Akiva-Tal et al., 2011).

In addition, in a complementary way, a set of GD (Retrosynthesis) crystallization experiments using the same biological gastrolith scaffolds were performed in order to stabilize gastrolithic ACC particles by using synthetic phytic (PA) acid, which has been reported as an efficient stabilizer of ACC particles (Xu et al., 2005) against crystallization in aqueous media. Therefore, in order to demonstrate the initial formation of ACC particles and the stabilizing role of PA, retrosynthesis mineralization through GD crystallization was performed. Fig. 7 shows the morphology of the $CaCO_3$ particles initially forming on the gastrogel (Fig. 7A) and sponge (Fig. 7B) matrices. Fig. 7A1 shows spherical aggregated ACC nanoparticles formed in the gastrogel matrix, with a size of 200–400 nm, whereas the electron diffraction pattern corroborates their amorphous character (Fig. 7A2). However, when the sponge was used as substrate, even smaller (<50 nm) ACC nanoparticles were observed (Fig. 7B1, Fig. 7B2 for the electron diffraction showing the amorphous character). Moreover, TEM analyses of $CaCO_3$ particles grown by the GD (Retrosynthesis) method with PA as additive on both matrices and in SF powdered solution after 3 days at room temperature were carried out (Supporting information, Fig. S2). ACC nanoparticles with sizes in the nanometer-range formed from minutes to days demonstrating that the stabilization capacity of the PA molecule in both biological gastrolith scaffolds was efficient. For instance, the PA additive in combination with the powdered SF matrix, which also contains P and PG biomolecules, showed an efficient capacity to induce spherical nanoparticles (Supporting information, Fig. S2 C).

Fig. 8 shows the XRD patterns of the $CaCO_3$ particles formed on the gastrogel (Fig. 8A) and sponge (Fig. 8C) matrices mineralized by the GD method after 15 min. XRD measurements were also performed after longer times of crystallization (3 days) of both gastrolith matrices, in which the formation of particles was evident (Fig. 8B and D). Fig. 8E shows the XRD pattern of the $CaCO_3$ particles grown when PA was used additive (control) at 3 days. The XRD patterns of $CaCO_3$ particles grown on both gastrolith scaffold

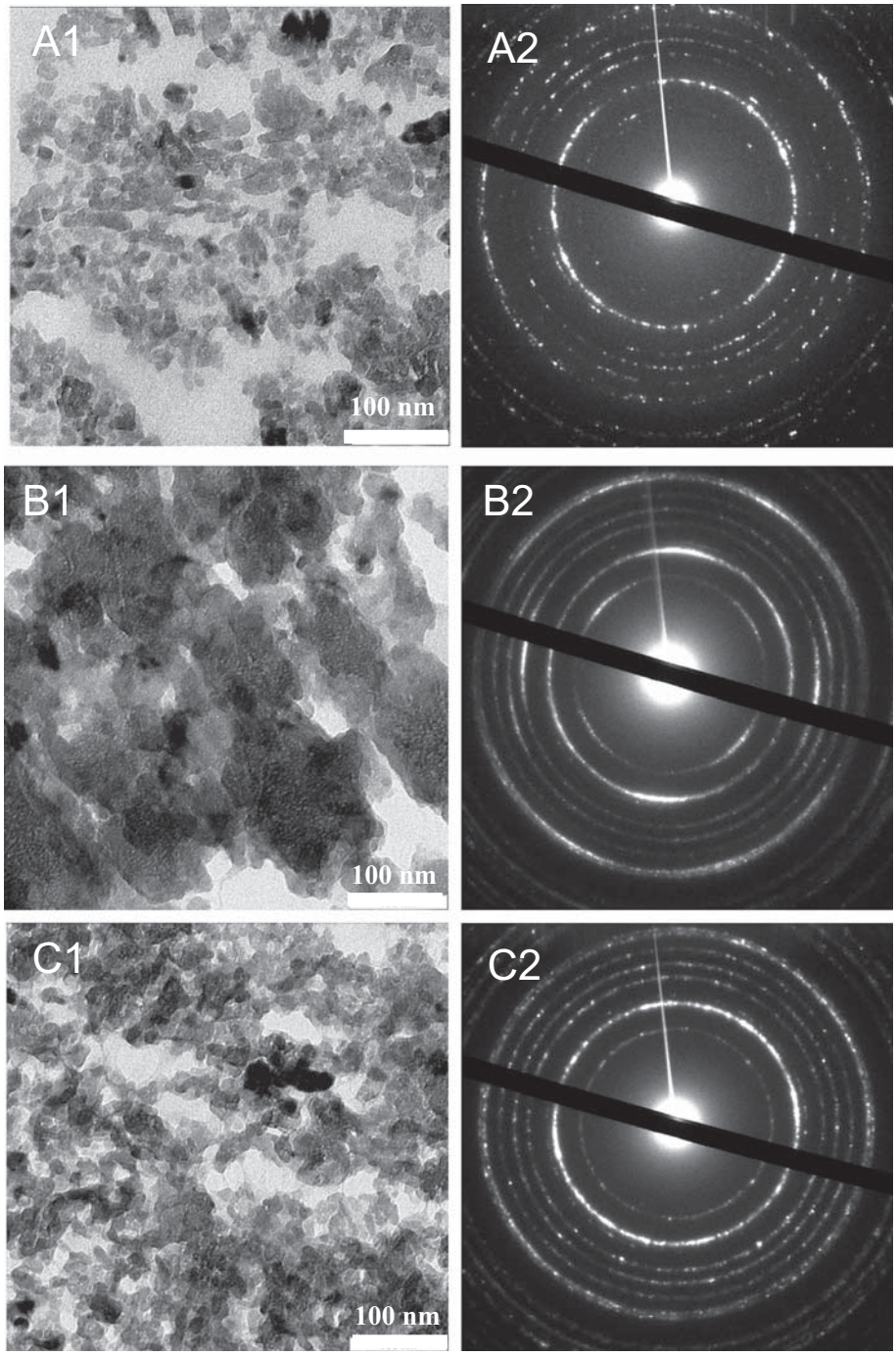

Fig. 6. TEM micrographs and electron diffraction patterns of $CaCO_3$ particles grown using DD (Retrosynthesis) with PAA after 8 days at room temperature. A) gastrolith, B) gastrogel, and C) sponge.

matrices are practically identical except for the unclear peaks at around $2\theta = 41°–43°$ and at $2\theta = 63.9°$, corresponding probably to $CaCl_2$ solution in which the PA was dissolved (Fig. 8C and D). Our experimental XRD spectra results showed no reflections attributable to a crystalline calcium carbonates, the resulting XRD patterns reveal some short- or medium-range order that may arise from the organic matrices, with clear amorphous volume fraction present in the sample, supporting the notion that the observed particles correspond to an amorphous $CaCO_3$ phase. The only clear peaks at $2\theta = 9°$ and in the range of at $2\theta = 19.1–19.8°$ are due to the presence of the organic chitin fiber molecules. However, when PA molecules were used as the only additive, no crystalline phase was determined and the two peaks at $2\theta = 7°$ and in the range of $2\theta = 26–28°$ are attributable to amorphous mineralized $CaCO_3$ particles (Fig. 8E). We rationalize that PA-induced stabilization of ACC particles at short times (15 min) in both gastrolith scaffold matrices and also at longer mineralization time (3 days), as described in the literature (Xu et al., 2005).

In order to complement the investigations of the role of the PA as unique soluble additive during the GD (Retrosynthesis) mineralization method, the effect of a lower concentration of PA (64 μg/ml) using a lower total volume of mineralization reac-

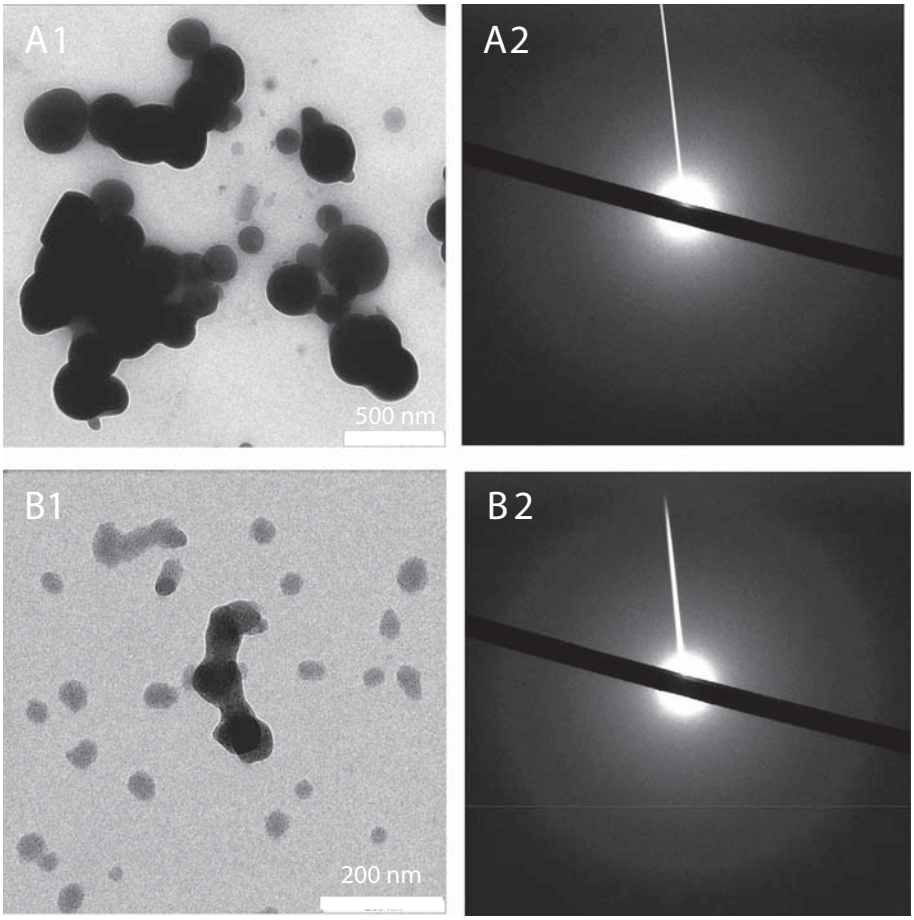

Fig. 7. TEM micrographs and electron diffraction patterns of $CaCO_3$ particles grown using the GD method with PA after 15 min mineralization time on A) gastrogel and B) sponge matrices.

tants (35 μL) for 24 h (Neira-Carrillo et al., 2005, 2009, 2012) was explored. XRD patterns of $CaCO_3$ particles grown in the presence of PA as additive, of the sponge matrix as solid scaffold, and the combination of sponge matrix with PA are shown in Fig. 9A–C, respectively. In the presence of PA, a unique crystalline peak is found at $2\theta = 31.7°$ corresponding to the calcite (006) face, which is not a predominant face in any $CaCO_3$ polymorphs. However, crystallization of $CaCO_3$ particles on the sponge matrix with or without PA showed a peak at $2\theta = 29.5°$ which is indicative of the (104) face of calcite. Therefore, the sponge matrix is able to influence the growth morphology and surface structure of calcite faces, and stabilizes, at this mineralization condition, crystalline forms of $CaCO_3$ masking the ACC stabilizing effect of PA.

This observation demonstrates that the synthetic PA molecule in the gastrolith scaffold matrices induces the formation of ACC particles, but this effect depends on PA concentration, time and type of mineralization. This can be rationalized by relative proportion of organic gastrolith scaffold and additive concentration and this scenario should be influences by the simultaneous presence of other biological macromolecules such as P, phosphoproteins, phosphorous-containing compounds (Sato et al., 2011; Habraken et al., 2015), sulfated GP, and polysaccharides, which inhibit the transformation of ACC to more stable crystalline polymorphs such as calcite or aragonite (Mann, 2001a,b; Arias et al., 2004). It is well known that most biogenic ACC deposits contain considerable quantities of magnesium and/or phosphorous, which are thought to play an important role in stabilizing ACC, as well. (Lowenstam and Weiner, 1989; Lowenstam, 1986; Dove et al., 2003; Donners et al., 2000; Luquet et al., 2016). In addition, we found that after a very long time of mineralization (21 days) employing the DD method and using PAA at room temperature, the initial ACC particles were transformed into calcite on the gastrogel matrix. Corresponding WAXS data demonstrating crystalline $CaCO_3$ particles grown on gastrogel matrix and the gastrogel used as control after 21 days of DD crystallization method can be found in the Supporting information (Fig. S3).

Therefore, light microscopy and ESEM micrographs of $CaCO_3$ particles grown on gastrolith matrix using GD method with PA at 15 min are in good agreement with the results obtained from XRD analyses outlined above. Microscopic analysis of $CaCO_3$ particles grown on both gastrolith matrices using the GD method with PA from minutes to days were performed (Supporting information, Fig. S2). In order to investigate the crystalline and amorphous zones across the intact gastrolith stone, a microfocus mapping across the gastrolith by SAXS analysis was performed at different positions (000–012) from the outside to the inner part of the gastrolith. The measurement positions of the gastrolith (stone embedded in PMMA support) and the corresponding space resolved X-ray scattering and SAXS ultrastructure analyses are visualized in the Supporting Information (Fig. S4). The small and wide-angle X-ray scattering (S/WAXS) data support the characterization outlined above, evidencing crystalline and amorphous zones across the gastrolith. The microfocus mapping results across the gastrolith with

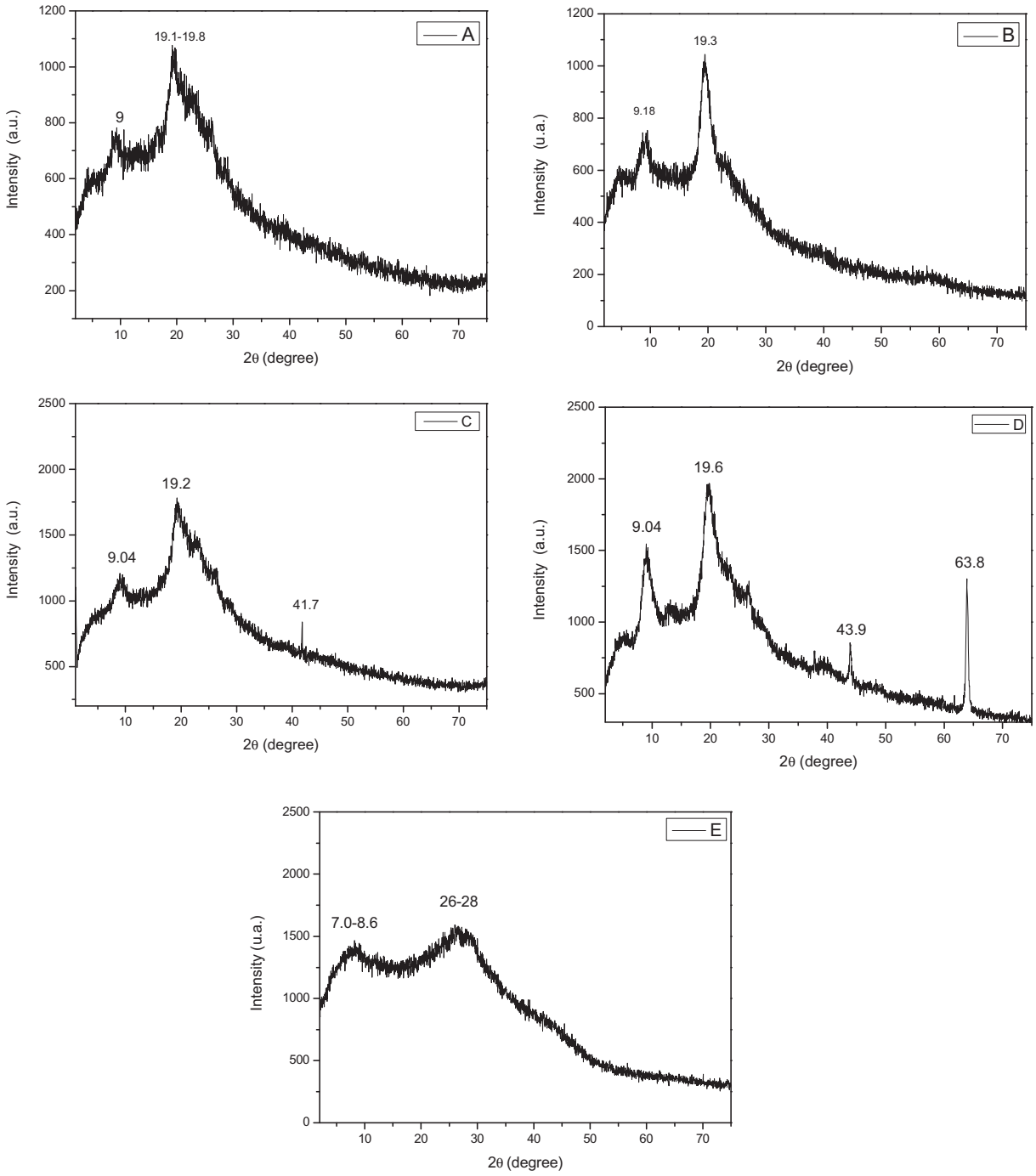

Fig. 8. XRD patterns of $CaCO_3$ particles grown using GD with PA on gastrolith matrices: A) gastrogel at 15 min, B) gastrogel at 3 days, C) sponge at 15 min, D) sponge at 3 days and E) PA as additive (control) at 3 days.

small angle X-ray scattering (SAXS) can be found in the Supporting information (Fig. S5).

In this context, Fig. 10 shows a summary of XRD and SAXS measurements carried out at two distinct positions in the gastrolith stone, which demonstrate the coexistence of a mixture of amorphous and crystalline (at position 012) and pure crystalline (at position 007) zones through the gastrolith. Standard reflections drawn as vertical lines in the diffractogram correspond to calcite (C), aragonite (A) and vaterite (V). The XRD spectrum for the position 012 (black curve) shows an intense broad reflex in the range of 2θ = 9.4–24.5° with a maximum at 2θ 15.5° indicating a large presence of an amorphous $CaCO_3$ phase. This XRD spectrum also showed a less intensity reflection peak at 2θ = 29.5° corresponding to the (104) reflection of calcite. The second XRD spectrum taken at the 007 position (green curve) shows a typical XRD diffractogram of calcite with the same and most intense reflection at 2θ = 29.5° attributed to the most intense (104) reflection of calcite. The correlation of XRD pattern taken at the 007 position and the calcite standard is very good. The reflection peak at 2θ = 42.7° can be attributed to vaterite. The occurrence of this polymorph may suggest that crystallization is triggered by sample preparation and thus could be an artefact.

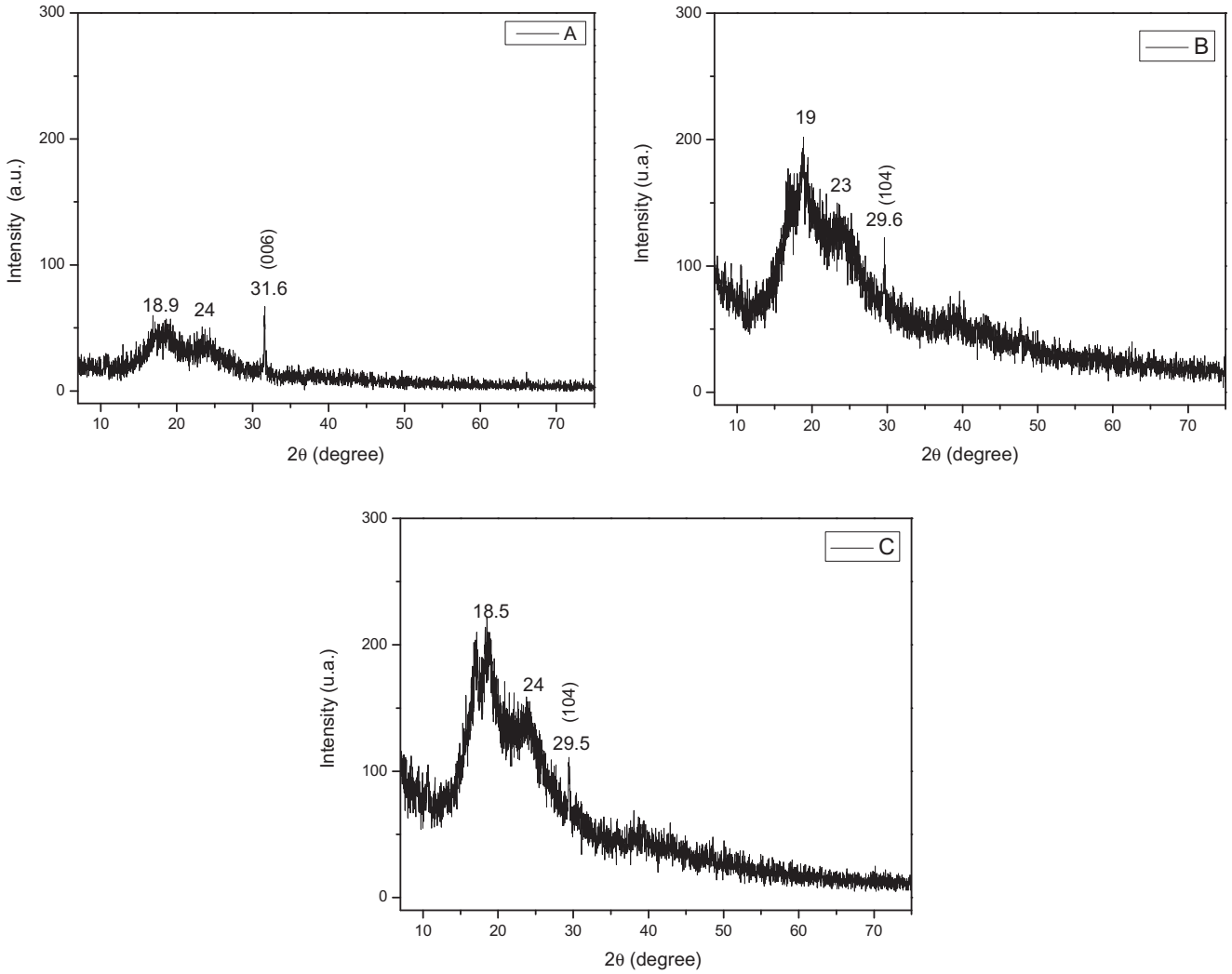

Fig. 9. XRD patterns of $CaCO_3$ particles grown using GD after 24 h in the presence of: A) PA as additive (control), B) sponge matrix (control), and C) sponge plus PA.

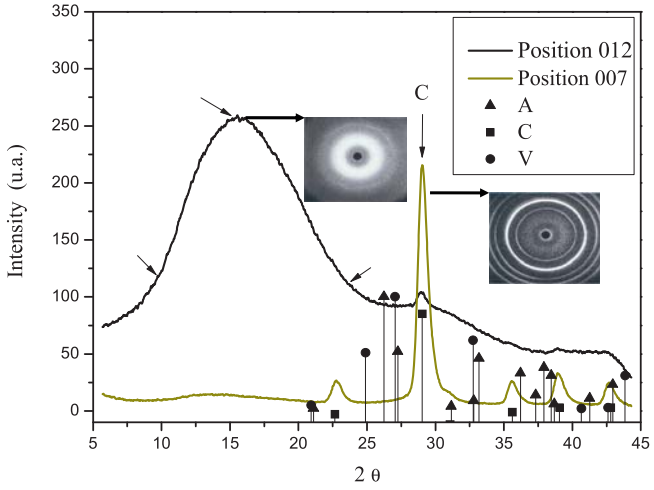

Fig. 10. XRD and SAWS analyses at two positions into the gastrolith demonstrating amorphous (at position 012, black curve) and crystalline (at position 007, green curve) zones. The three types of vertical lines correspond to reflection patterns of standards of calcite (C), aragonite (A) and vaterite (V).

4. Conclusions

We report the feasibility to use a biomimetic retrosynthetic approach for the mineralization of gastrolith scaffolds as a confined environment via amorphous precursor particles. This study suggests that in nature, the gastrolith stone of the Red Claw Lobster (*Cherax quadricarinatus*) is mineralized analogically. We demonstrated using DD and GD crystallization methods that distinct fractions of the IF, that is, the gastrogel and sponge matrices, can be mineralized in combination with PAA and PA acid molecules, which can effectively control the morphogenesis and the crystallographic polymorphism of $CaCO_3$ intermediate nanoparticles. The results of the current retrosynthesis approach utilized various characterization techniques, which were in good agreement with the natural lobster structures, thus supporting the notion of the realization of a biomimetic retrosynthesis of $CaCO_3$ particles. Optical and SEM analyses showed different $CaCO_3$ morphologies confirming that ACC precursor particles are required to obtain crystalline minerals that mimic their biological counterparts. Light microscopy demonstrated the formation of $CaCO_3$ particles in real time through the DD diffusion method. XRD and electron diffraction demonstrated the occurrence of stabilized ACC particles and the importance of proteins and PG molecules as well as phosphorous-containing compounds within the gastrolith scaffold

when it comes to the stabilization of ACC. In summary, the biomimetic retrosynthetic approach reported herein offers a wide range of possibilities for the controlled generation of organic/inorganic hybrid composite materials with defined morphologies.

Acknowledgments

This research was supported by FONDECYT N° 1140660 & 11070136 granted by the Chilean Council for Science and Technology (CONICYT). Dr. Neira-Carrillo would like to thank Prof. Markus Antonietti (MPI of Colloids and Interfaces, Golm, Potsdam, Germany) for providing equipment facilities. DG is a Research Fellow of the Zukunftskolleg of the University of Konstanz.

References

Akiva-Tal, A., Kababya, S., Balazs, Y.S., Glazer, L., Berman, A., Sagi, A., Schmidt, A., 2011. In situ molecular NMR picture of bioavailable calcium stabilized as amorphous $CaCO_3$ biomineral in crayfish gastroliths. PNAS 10, 14763–14768.

Arias, J.L., Fernández, M.S., 2008. Polysaccharides and proteoglycans in calcium carbonate-based biomineralization. Chem. Rev. 108, 4475–4482.

Arias, J.L., Carrino, D.A., Fernández, M.S., Rodríguez, J.P., Dennis, J.E., Caplan, A.I., 1992. Partial biochemical and immunochemical characterization of avian eggshell extracellular matrices. Arch. Biochem. Biophys. 298, 293–302.

Arias, J.L., Neira-Carrillo, A., Arias, J.I., Escobar, C., Bodero, M., David, M., Fernández, M.S., 2004. Sulfated polymers in biological mineralization: a plausible source for bio-inspired engineering. J. Mater. Chem. 14, 2154–2160.

Bäuerlein, E., 2003. Biomineralisation von Einzellern: eine außergewöhnliche Membranbiochemie zur Produktion anorganischer Nano- und Mikrostrukturen. Angew. Chem. 115, 636–664.

Bentov, S., Weil, S., Glazer, L., Sagi, A., Berman, A., 2010. Stabilization of amorphous calcium carbonate by phosphate rich organic matrix proteins and by single phosphoamino acids. J. Struct. Biol. 171, 207–215.

Cölfen, H., 2003. Precipitation of carbonates: recent progress in controlled production of complex shapes. Curr. Opin. Colloid Interface Sci. 8, 23–31.

Cölfen, H., Mann, S., 2003. Geordnete mesoskopische Strukturen durch Selbstorganisation und transformation von Hybrid-Nanostrukturen. Angew. Chem. 115, 2452–2468.

Domínguez-Vera, J.M., Gautron, J., García-Ruiz, J.M., Nys, Y., 1999. The effect of avian uterine fluid on the growth behavior of calcite crystals. Poultry Sci. 79, 901–907.

Donners, J.J.J.M., Heywood, B.R., Meijer, E.W., Nolte, R.J.M., Roman, C., Schenning, A. P.H.J., Sommerdijk, N.A.J.M., 2000. Amorphous calcium carbonate stabilised by poly(propylene imine) dendrimers. Chem. Commun. 19, 1937–1938.

Dove, P.M., De Yoreo, J.J., Weiner, S., 2003. Biomineralization. Rev. Mineral. Geochem. 54, 381.

Fabritius, H., Walther, P., Ziegler, A., 2005. Architecture of the organic matrix in the 697 sternal $CaCO_3$ deposits of *Porcellio scaber* (Crustacea, Isopoda). J. Struct. Biol. 150, 190–199.

Fernández, M.S., Bustos, C., Luquet, G., Saez, D., Neira-Carrillo, A., Corneillat, M., Alcaraz, G., Arias, J.L., 2012. Proteoglycan occurrence in gastrolith of the crayfish *Cherax quadricarinatus* (Crustacea, Malacostraca, Decapoda). J. Crustacean Biol. 32, 802–815.

Gebauer, G., Cölfen, H., Verch, A., Antonietti, A., 2009. The multiple roles of additives in $CaCO_3$ crystallization: a quantitative case study. Adv. Mater. 21, 435–439.

Gehrke, N., Nassif, N., Pinna, N., Antonietti, M., Gupta, H.S., Cölfen, H., 2005. Retrosynthesis of nacre via amorphous precursor particles. Chem. Mater. 17, 6514–6516.

Habraken, W.J.E.M., Masic, A., Bertinetti, L., Al-Sawalmh, A., Glazer, L., Bentov, S., Fratzl, P., Sagi, A., Aichmayer, B., Berman, A., 2015. Layered growth of crayfish gastrolith: about the stability of amorphous calcium carbonate and role of additives. J. Struct. Biol. 189, 28–36.

Lowenstam, H.A., 1986. Mineralization process in monerans and protoctists. In: Riding, R. (Ed.), Biomineralization in Lower Plants and Animals. Leadbeater BSC, 30. Oxford University Press, New York, p. 1.

Lowenstam, H.A., Weiner, S., 1989. On Biomineralization. Oxford Univ. Press, Oxford.

Luquet, G., Marin, F., 2004. Biomineralisations in crustaceans: storage strategies. C. R. Palevol. 3, 515–534.

Luquet, G., Fernández, M.S., Badou, A., Guichard, N., Le Roy, N., Corneillat, M., Alcaraz, G., Arias, J.L., 2013. Comparative ultrastructure and carbohydrate composition of gastroliths from astacidae, cambaridae and parastacidae freshwater crayfish (Crustacea, Decapoda). Biomolecules 3, 18–38.

Luquet, G., Dauphin, Y., Percot, A., Salomé, M., Ziegler, A., Fernández, M.S., Arias, J.L., 2016. Calcium deposits in the crayfish, *Cherax quadricarinatus*: microstructure versus elemental distribution. Microsc. Microanal. 22, 22–38.

Mann, S., 1996. Biomimetic Materials Chemistry. VCH, Wheinheim, p. 383.

Mann, S., 2001a. Biomineralization, Principles and Concepts in Bioinorganic Materials Chemistry. Oxford University Press.

Mann, S., 2001b. In: Compton, R.G., Davies, S.G., Evans, J. (Eds.), Biomineralization. Oxford University Press, Oxford.

Mann, S., Ozin, G.A., 1996. Synthesis of inorganic materials with complex form. Nature 382, 313–318.

Meldrum, F.C., 2003. Calcium carbonate in biomineralisation and biomimetic chemistry. Int. Mater. Rev. 48, 187–224.

Neira-Carrillo, A., Yazdani-Pedram, M., Retuert, J., Diaz-Dosque, M., Gallois, S., Arias, J.L., 2005. Selective crystallization of calcium salts by poly(acrylate)-grafted chitosan. J. Colloid Interface Sci. 286, 134–141.

Neira-Carrillo, A., Pai, R.K., Fernández, M.S., Carreño, E., Vasquez-Quitral, P., Arias, J. L., 2009. Synthesis and characterization of sulfonated polymethylsiloxane polymer as template for crystal growth of $CaCO_3$. Colloid Polym. Sci. 287, 385–393.

Neira-Carrillo, A., Vasquez-Quitral, P., Díaz, M.P., Fernández, M.S., Arias, J.L., Yazdani-Pedram, M., 2012. Control of calcium carbonate crystallization by using anionic polymethylsiloxanes as templates. J. Solid State Chem. 194, 400–408.

Ozin, G.A., 1997. Morphogenesis of biomineral and morphosynthesis of biomimetic forms. Acc. Chem. Res. 30, 17–27.

Pai, R.K., Pillai, S., 2008. Nanoparticles of amorphous calcium carbonate by miniemulsion: synthesis and mechanism. CrystEngComm 10, 865–872.

Pereira-Mouriès, L., Almeida, M.J., Ribeiro, C., Peduzzi, J., Barthélemy, M., Milet, C., Lopez, E., 2002. Soluble silk-like organic matrix in the nacreous layer of the bivalve Pinctada maxima. Eur. J. Biochem. 269, 4994–5003.

Raz, S., Testeniere, P., Hecker, A., Weiner, S., Luquet, G., 2002. Stable amorphous calcium carbonate is the main component of the calcium storage structures of the crustacean *Orchestia cavimana*. Biol. Bull. 203, 269–274.

Sato, A., Nagasaka, S., Furihata, K., Nagata, S., Arai, I., Saruwatari, K., Kogure, T., Sakuda, S., Nagasawa, H., 2011. Glycolytic intermediates induce amorphous calcium carbonate formation in crustaceans. Nat. Chem. Biol. 7, 197–199.

Saw, N.K., Chow, K., Rao, P.N., Kavanagh, J.P., 2007. Effects of inositol hexaphosphate (Phytate) on calcium binding, calcium oxalate crystallization and in vitro stone growth. J. Urol. 177, 2366–2370.

Shechter, A., Berman, A., Singer, A., Freiman, A., Grinstein, M., Erez, J., Aflalo, E.D., Sagi, A., 2008. Reciprocal changes in calcification of the gastrolith and cuticle during the molt cycle of the red claw crayfish *Cherax quadricarinatus*. Biol. Bull. 214, 122–134.

Travis, D.F., 1963. Structural features of mineralization from tissue to macromolecular levels of organization in the decapod crustacea. Ann. N. Y. Acad. Sci. 109, 177–245.

Volkmer, D., Harms, M., Gower, L., Ziegler, A., 2005. Morphosynthesis of nacre-type laminated $CaCO_3$ thin films and coatings. Angew. Chem. Int. Ed. 44, 639–644.

Weiner, S., Addadi, L., 1991. Acidic macromolecules of mineralized tissues: the controllers of crystal formation. Trends Biochem. Sci. 1991 (16), 252–256.

Xu, A.-W., Yu, Q., Dong, W.-F., Antonietti, M., Cölfen, H., 2005. Stable amorphous $CaCO_3$ microparticles with hollow spherical superstructures stabilized by phytic acid. Adv. Mater. 17, 2217–2221.

Yanagishita, M., Hascall, V.C., 1983. Characterization of heparan sulfate proteoglycans synthesized by rat ovarian granulosa cells in culture. J. Biol. Chem. 258, 12857–12864.

Ziegler, A., 1994. Ultrastructure and electron spectroscopic diffraction analysis of the sternal calcium deposits of *Porcellio scaber* Latr. (Isopoda, Crustacea). J. Struct. Biol. 112, 110–116.